Food Physics 2 (2025) 100028

Contents lists available at ScienceDirect

Food Physics

journal homepage: www.keaipublishing.com/en/journals/food-physics/

# Simulated construction of plant-based fish meat with composite structure via dual-nozzle extrusion 3D printing

Jie Li[a,b], Haohao Hu[a,b], Ruihao Niu[a], Qingqing Zhu[a,b], Siyu Yao[a], Jianwei Zhou[b,c], Donghong Liu[a,b], Enbo Xu[a,b,*]

[a] College of Biosystems Engineering and Food Science, National Engineering Laboratory of Intelligent Food Technology and Equipment, the State Key Laboratory of Fluid Power and Mechatronic Systems, Zhejiang Key Laboratory for Agro-Food Processing, Fuli Institute of Food Science, Zhejiang University, Hangzhou 310058, China
[b] Innovation Center of Yangtze River Delta, Zhejiang University, Jiaxing 314102, China
[c] School of Mechanical and Energy Engineering, NingboTech University, Ningbo 315100, China

ARTICLE INFO

*Keywords:*
Fish tissue simulation
Plant-derived product
3D printing precision
Multi-outlet extrusion
Customized food

ABSTRACT

Three-dimensional (3D)-printed fish analogs are gradually nearing the ability to mimic real fish meat in response to personal demand, supply pressure, food safety, and environmental concerns. However, the use of 3D food printing to simulate the composite structure of real meat tissue remains a challenge. In this study, we used dual-nozzle 3D printing technology to construct plant-based yellow croaker tissue analogs by soy protein isolate–xanthan gum-starch complex (as simulated muscle ink) and nanostarch-carrageenan emulsion gel (as simulated fat ink). We successfully prepared 3D-printed fish meat with a high simulation composite structure by constructing a muscle/fat biphasic 3D model and optimizing the printing process. The texture, moisture distribution, and nutrient content of the simulated fish meat were analyzed and compared with real yellow croaker meat, demonstrating that 3D-printed plant-based yellow croaker flesh with a composite structure had a good simulation quality.

## 1. Introduction

According to an estimation made by the Food and Agriculture Organization of the United Nations (FAO), 140 million tons of fish will be consumed worldwide by 2050 [1]. Further, according to Anderson et al., [2] prior assessment, about 90 % of fish resources worldwide have already reached their sustainable fishery limit. High-density aquaculture (also known as industrialized aquaculture) enables, by means of technology and artificial control, more aquatic life to be planted in a smaller area and water body [21]. While high-density farming and aquaculture help to meet the increasing demand for seafood, they also cause significant pollution and harm to the environment. Eriksen et al. [5] reported that there are 5.25 trillion plastic particles in the world's oceans, and they may even be detected in deep water and in marine life near the North and South Poles. To solve the problems of insufficient production efficiency and environmental deterioration, plant-based fish mimics have thus arisen as one of the competitive alternatives to traditional fisheries.

* Corresponding author at: College of Biosystems Engineering and Food Science, National Engineering Laboratory of Intelligent Food Technology and Equipment, the State Key Laboratory of Fluid Power and Mechatronic Systems, Zhejiang Key Laboratory for Agro-Food Processing, Fuli Institute of Food Science, Zhejiang University, Hangzhou 310058, China
*E-mail addresses:* enbo_xu@163.com, enboxu@zju.edu.cn (E. Xu).

https://doi.org/10.1016/j.foodp.2024.100028
Received 5 July 2024; Received in revised form 19 August 2024; Accepted 1 September 2024
Available online 5 September 2024

Recently, the cutting-edge technology of three-dimensional (3D) food printing has shown numerous advantages, such as the capacity to achieve personalized diets, customized structures, and optimized supply chains [19]. With the continuous development of the personalized food market, demand for the multi-component and multi-layer composite structure design of food products is emerging, such as multi-phase simulation of plant meat products and a hierarchal food/medicine structure with a slow release of ingredients. Dual-nozzle or coaxial 3D printing technologies can simultaneously conduct printing with two different inks by regulating the nature of the substrate, optimizing the print path, and adjusting the synergistic parameters. Several researchers have focused on coaxial printing and dual-nozzle printing in the design and production of plant meat. For example, Ko et al. [8] used soybean isolate protein and potato starch as the main materials, and utilized the cross-linking principle of calcium ions and sodium alginate to insert carrageenan-based hydrocolloids artificially by using coaxial printing to prepare simulated chicken meat with a fibrous texture. Wang et al. [17] utilized dual-nozzle printing to prepare surimi analogs with two different colors of high internal-phase emulsions, though low precision and a rough printing surface were challenges. Thus far, research on 3D printing tailored composite structures of meat analogs is minimal, and much is still in the primary stage. In addition, there are processing issues with dual-nozzle 3D printing, including poor material and nozzle matching, repetitious printing paths, and low printing accuracy.

In previous studies, our team developed soy protein isolate-rice starch–xanthan gum complexes for a high-precision fiber structure of muscle analogs [14,9]. In addition, nanostarch (NS)-enhanced emulsion gels for the high-precision print control of fat analogs were developed. The formulation, preparation method, optimization process, data characterization, and results discussion of these two printing inks were successfully detailed. As well, the above food inks were utilized to prepare a plant-based fish meat using printable raw materials by high-precision dual-nozzle printing technology. This process of dual-nozzle printing plant-based fish mainly involves the following steps: 1) constructing muscle/fat biphasic 3D models, 2) optimizing the printing process (manual calibration of dual-nozzle offset, layer height, fill rate, dual-nozzle printing speeds, dual-nozzle printing air pressures, and print path setting, etc.). Comparative analyses of the nutrient composition, moisture state, and texture of the simulated fish flesh obtained from dual-nozzle printing and real yellow croaker flesh were performed, and it was found that the simulated fish tissue had a high degree of biofidelity.

## 2. Materials and methods

### 2.1. Materials

Previous studies [14,9] offered a detailed description of and introduction to the materials. In brief, Shanghai Macklin Biochemical Co., Ltd. (China) supplied soy protein isolate (SPI, content ≥ 90 %, analytical grade). Shanghai Yuanye Bio-Technology Co., Ltd. (China) supplied rice starch (RS), and the supplier of xanthan gum (XG) was Tianjin HEOWNS Biochem Technologies Co., Ltd. in China. The characteristics of fish analogs were contrasted from those of yellow croakers, which were imported from a Walmart supermarket and reared in China. Native corn starch was provided by Karl Golden, a company located in Hangzhou, China. Sinopharm Chemical Reagent Co., Ltd. (Hangzhou, China) provided the absolute ethanol, and we purchased sodium hydroxide from Sigma-Aldrich in St. Louis, Missouri, USA. The supplier of the carrageenan (CG, iota Carrageenan, commercial grade, type II) was Sigma in Shanghai, China, and the soybean oil was purchased from a nearby store without any additional processing. We purchased fish oil from Xian Dongchi Biological Technology Co., Ltd. (Xi'an, China), which contained 50 % docosahexaenic acid (DHA). Every other chemical was of an analytical variety.

### 2.2. Micro-CT scan of yellow croaker tissue

To explore fully the differences in the native structure of yellow croaker muscle tissue, three large areas (dorsal, abdominal, and caudal parts) of the edible portion of fish flesh were sampled separately. Among them, the back parts of muscle groups were more numerous, and three areas were sampled, namely, at the spine, the anterior dorsal muscles, and the posterior dorsal muscles. The abdominal region sampled the fundus abdominis muscles and the middle region of the abdomen, and the tail region was sampled at only one site due to the small number of edible parts. As shown in Fig. 2**a**, the sampling sites included the dorsal flesh (S1), the front part of the dorsal flesh, the latter part of the dorsal flesh, the belly, the base of the belly flesh (S2), and the tail (S3), for a total of six muscle tissue sites.

Referring to the method of Zhu et al. [22] with some modifications, as well as sample processing and staining, after thawing the chilled yellow croaker purchased from the market and removing the fish scales, different parts of the flesh samples were cut, and the samples were immersed in 4 % (v/v) paraformaldehyde for fixation for 8 h [7]. Configuration of the 3.75 % iodine-potassium iodide solution is as follows: 5 g of iodine monomers and 10 g of potassium iodide were dissolved in 100 mL of distilled water, mixed well, and then diluted four times. The fixed yellow croaker muscle specimens were continuously immersed with 3.75 % compound iodine solution for 14 d, and the samples were washed with distilled water and 75 % alcohol to remove the excess iodine solution after immersion was complete.

Micro-CT scanning: CT scans were performed with a Micro-CT bioscanner (SkyScan1272, Bruker Co., Ltd., Germany) under the following conditions: source voltage = 100 kV, source current = 100 μA, exposure time = 1738 ms, scaled image pixel size = 10 μm, and 360° rotational scanning. Referring to the method of Zhu et al. [22], micro-CT slice data were imported into the Avizo image processing software (Avizo 2019, Thermo Fisher Scientific, USA), coarse filtering was performed using the anisotropic diffusion mode, and the background detection correction mode was altered to adjust color homogenization and remove small spots, which functions to remove small noise. After pre-processing the CT image data, the volume rendering and the interactive thresholding modes are selected to divide the threshold manually, and the model can be divided into muscle and fat parts to generate the visualization model.

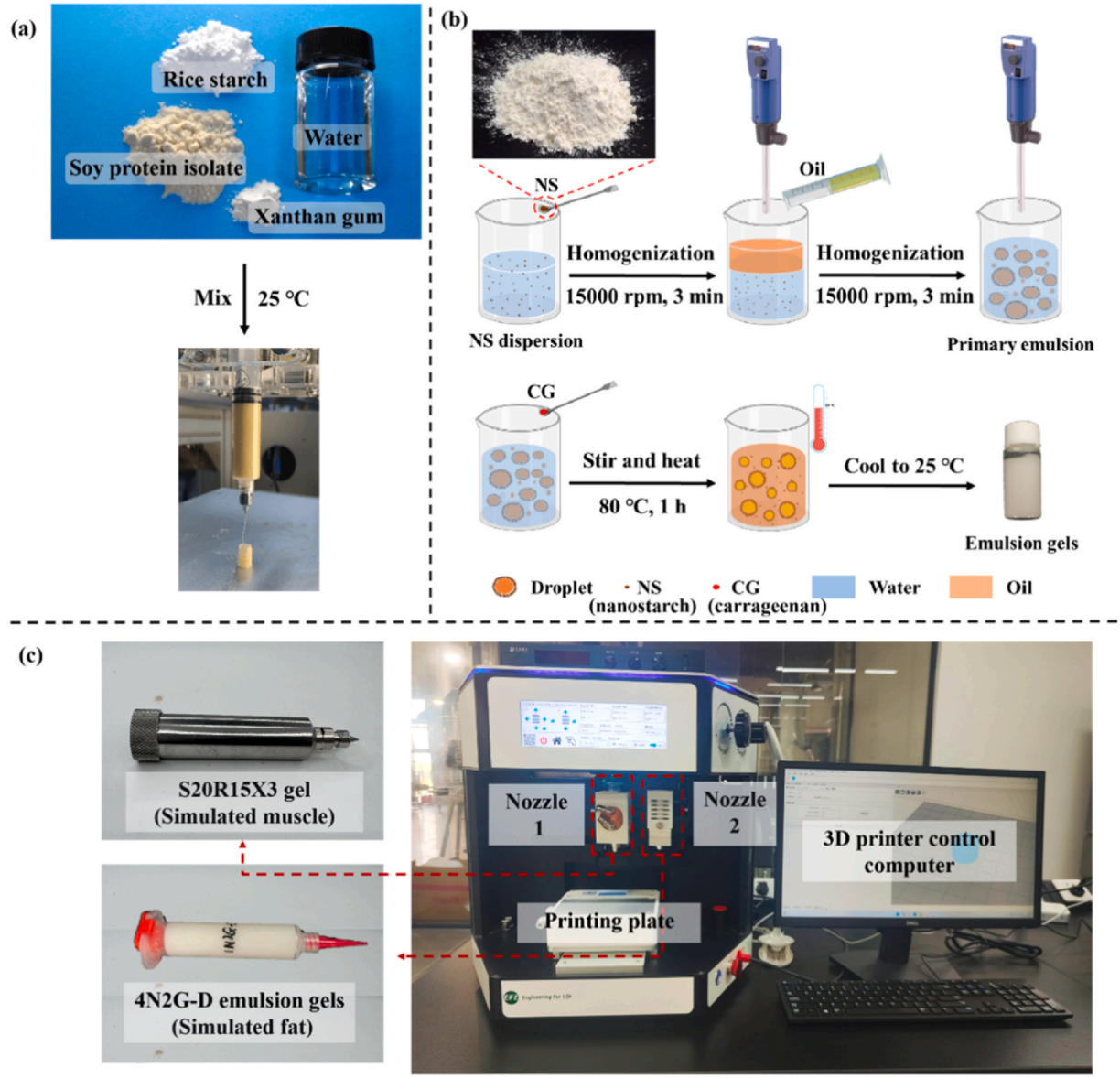


**Fig. 1.** Printing materials and operating procedure of dual-jet 3D printing system [14,9]. (a) Preparation of S20R15X3 gel (printing ink for simulated muscle); (b) Preparation of 4N2G-D emulsion gels (printing ink for simulated fat); (c) Schematic of the 3D extrusion printing system.

### *2.3. Preparation of SPI/XG/RS composite gels*

As described in Fig. 1a, the SPI/XG/RS composite gels used for the plant-based simulation of yellow croaker muscle parts was prepared from soybean isolate protein, rice starch, and xanthan gum. To imitate the muscular section of yellow croaker flesh, we used the S20R15X3 complex (SPI concentration of 20 wt%, RS concentration of 15 wt%, and XG concentration of 3 wt%), which provided the best modeling effect of printing. SPI and XG were initially combined for 5 min, after which deionized water was added and the mixture was agitated for 20 min at 25℃ to obtain an ink in good print condition. Subsequently, RS were included into the SPI/XG blend, and the combined mixture was kneaded for approximately 30 min until a macroscopically consistent paste (S20R15X3 complex gel) was formed.

### *2.4. Preparation of nanostarch–carrageenan emulsion gels*

The NS particles were prepared according to our team's previous works [13,9]. The T 18 brushless digital ULTRA-TURRAX homogenizer (IKA, Staufen, Germany) was used for synthesis of the NS particles, which was dissolved with 5 g of starch powder (10–30 μm) under high-speed homogenization (3000 rpm) to create a fully gelatinized 5 % (w/v) native corn starch paste.

Subsequently, to nucleate and create NS quickly, 100 mL of starch paste was injected dropwise into 100 mL of 100 % ethanol while being homogenized at a high speed (15,000 rpm) for 5 min. To obtain the NS precipitate, the mixtures were centrifuged at 2000 × g for 10 min, and after being washed with pure ethanol, the mixture was dried at 50 ℃ for 6 h. Then, it was ground to a powder and sieved through a 200-mesh sieve.

Based on Fig. 1b, the NS-carrageenan (NS–CG) emulsion gels were made with the T 18 brushless ULTRA-TURRAX homogenizer (IKA, Staufen, Germany). To ensure the NS particles (4 % w/v, NS solutions) were evenly distributed throughout the system, they were dissolved in water and homogenized at 15,000 rpm for 3 min. Meanwhile, to create an NS-stabilized emulsion, 20 % DHA-rich fish oil was then added and homogenized for 3 min at a speed of 15,000 rpm. The NS-stabilized emulsion was supplemented with the CG powers (2 % in the system), and after exposure to 70 ˚C for 1 h, the emulsion gels were allowed to cool to room temperature. That is, 4N2G-D emulsion gels show that the concentration of CG in the emulsion gel was 2 % and the concentration of NS in the starch solution was 4 %.

### 2.5. Low-field nuclear magnetic resonance

The sample test was conducted using low-field nuclear magnetic resonance (LF NMR), where the relaxation times ($T_2$) of the samples were determined using a nuclear magnetic resonance analyzer (NMI20–015 V-I, Niumag Co., Ltd., Shanghai, China) equipped with a 0.5-T permanent magnet, which is equivalent to a proton resonance frequency of 21.16 MHz at 32 ˚C. In short, each sample weighed 20 g, was wrapped in a thin plastic film, and then inserted into a 40 mm glass tube for measurement. The spin-spin relaxation time $T_2$ was determined using Carr–Purcell–Meiboom–Gill (CPMG) sequences with the following parameters: time waiting ($T_W$) = 10,000 ms, time echo ($T_E$) = 0.55 ms, number of echoes (NECH) = 18,000, and number of scans (NS) = 4. Then, the MultiExp Inv Analysis 4.09 (Niumag Electric Co., Ltd., Shanghai, China) software was used to analyze the data using both the mono- and multi-exponential fitting of $T_2$ relaxation data. For every measurement, there were three replications.

### 2.6. Texture profile analysis

Referring to the methodology of previous studies [14], using a flat-surface cylindrical probe (36 mm in diameter), the 3D printed simulated yellow croaker tissues were analyzed using a texture analyzer (Universal TA, Shanghai Tengba Instrument Co., Ltd., Shanghai, China). After the samples were put on the texture analyzer testing platform, the undisturbed samples were compressed by the probe for five seconds at a rate of 1.00 mm/s to a depth of 30 % of the sample height). Gram force was used to represent the force unit, and three duplicate samples were used for the measurements, all at room temperature.

### 2.7. Nutrition analysis

Crude fat was determined according to the Chinese national standard GB 5009.6–2016, crude protein content was determined according to the Chinese national standard GB 5009.5–2016, a fatty acid analysis was performed according to the Chinese national standard GB 5009.168–2016, and an amino acid analysis was performed according to the Chinese national standard GB 5009.124–2016. Analyses of the fatty acid and amino acid compositions of the prepared simulated fish tissues were compared with those of real yellow croaker fish.

### 2.8. 3D printing process

A dual-nozzle extrusion 3D printer (EFL 6602 Pro, EFL Tech Co., Ltd., Suzhou, China) was used to print composite structured plant-based simulated yellow croaker fish tissues. As illustrated in Fig. 1c, the system comprises a three-axis positioning stage with a working space of 10 × 10 × 5 cm and automatic motions along the X, Y, and Z axes to control the motion of the receiving platform and the nozzle. Two 10-mL syringes were filled with the edible inks (nozzle 1 for simulated muscle and nozzle 2 for simulated fat), and the 3D printing procedure was performed at room temperature the entire time. Table 1 is a list of printing parameters.

S1\S2\S3 models (S1-dorsal flesh; S2-the base of the belly flesh; S3-the tail flesh) with the following parameters were used as print models in the dual-nozzle printing experiments: the S1 model with a 2.00-mm height (Z), 3.60-cm length (X), and 4.26-cm width (Y);

**Table 1**
Parameters related to the dual-nozzle 3D printing experiment (nozzle 1 for simulated muscle and nozzle 2 for simulated fat).

| Parameter | Value |
|---|---|
| Print fill rate (%) | 70 |
| Printing layer height (μm) | 400 |
| Nozzle inner diameter of nozzle 1 (μm) | 600 |
| Nozzle inner diameter of nozzle 2 (μm) | 260 |
| Air pump pressure of nozzle 1 (kPa) | 160–250 |
| Air pump pressure of nozzle 2 (kPa) | 10–25 |
| XY moving speed of nozzle 1 (mm/min) | 660 |
| XY moving speed of nozzle 2 (mm/min) | 900 |

the S2 model with a 2.00-mm height (Z), 1.24-cm length (X), and 4.84-cm width (Y); the S3 model with a 2.00-mm height (Z), 1.85-cm length (X), and 4.41-cm width (Y). Measuring the length of the printed product in the X, Y, and Z directions with vernier calipers will enable the calculation of printing accuracy and the printing deformation rate.

Eq. (1) was used to compute the deformation rate [9], where a printed product is said to be expanding if its value is more than 0 and contracting if its value is less than 0.

$$Deformation\ rate = \frac{L_s - L_m}{L_m} \tag{1}$$

where $L_s$ is the 3D-printed sample's actual length (in mm) along one of the XYZ directions. $L_m$ is the model's fixed length (mm) along one of the XYZ directions.

Using Eq. (2), the total printing precision was determined:

$$Printing\ precision(\%) = \frac{\left(1 - \frac{|X_s - X_m|}{X_m}\right) + \left(1 - \frac{|Y_s - Y_m|}{Y_m}\right) + \left(1 - \frac{|Z_s - Z_m|}{Z_m}\right) \times 100\%}{3} \tag{2}$$

The length of the 3D-printed sample in the X-direction is denoted by $X_s$ (mm). The 3D-printed sample's length (mm) in the Y direction is denoted by the symbol $Y_s$, and $Z_s$ is the 3D-printed sample's length (in millimeters), measured in the Z-direction. The set length (mm) in the model's X-direction is represented by $X_m$, while the set length (mm) in the Y-direction of the model is represented by $Y_m$. In the Z-direction of the model, $Z_m$ stands for the specified length (mm).

### 2.9. Statistical analysis

Each test was performed in triplicate. GraphPad Prism 8 was used to graph, and data analyses were performed using the Statistical Package for the Social Sciences (SPSS 24, IBM). Differences of $p < 0.05$ with Tukey's test were considered significant.

## 3. Results and discussion

### 3.1. Micro-CT scanning and analysis of yellow croaker flesh

The results of the six-part micro-CT scan are shown in Fig. 2b, where the 3D reconstruction of the CT data at the spine can be clearly observed, with the muscle distinguished from the septum (mainly connective tissue). In addition, in the lateral model view, muscle fiber bundles arranged along a diagonal line can be discerned. A report by Hiran [6] showed that the supra-axial muscles of the trunk and caudal regions do not differ significantly in construction except for in size, whereas the infra-axial muscles trunk and caudal regions differ significantly in construction due to the presence of the abdominal cavity, as shown at the base of the abdomen in Fig. 2b-v. Here, the infra-axial muscles of the abdomen are only thinly packed, and the outer dark black portion of the infra-axial muscles are connective tissues (fats). Meanwhile, the musculature of the caudal part of the fish shows a concentric circular structure typical of fish cross-sections (Fig. 2b-vi).

The three dorsal muscles sampled (the dorsal flesh, the front part of the dorsal flesh, the latter part of the dorsal flesh) were similar in basic structure, except for a slight difference in fat/muscle ratios; therefore, only the muscles at the dorsal spine were chosen to represent the dorsal muscles in the subsequent study. Similarly, the scanning results at the base of the belly flesh emphasized better the specificity of the abdominal tissue structure; thus, the base of the belly flesh was used to represent the abdominal tissue. As such, further experiments were mainly based on samples from three areas: the dorsal flesh (S1), the base of the belly flesh (S2), and the tail (S3).

### 3.2. Construction of the muscle/fat composite printing model

A two-component rendering model can be obtained by selecting the appropriate rendering color for observing the tissue structure of the fish flesh (Fig. 3a). Based on the two-component rendering model, a 3D model of the micro-CT scan data was generated (Fig. 3b). The image data were first pre-cut by cutting the subject separately, so its adjustment range did not include the peripheral shadows. Then, the beam hardening correction function was used to correct the anomalous darkness in the model's center region (Fig. 3b-ii). The "Generate surface" mode was used to generate a surface mesh for the samples, and the data were exported as a Standard Triangle Language (STL) file, which could be used for 3D printing. However, it was found that the software could not slice the model due to the large amount of model data (13 G), which exceeded the software load. Therefore, it could not be used directly for the 3D printing experiments, and model optimization was performed in the following steps.

Because the whole piece of fish tissue was scanned for the model and the data were too large for recognition, the sample was cut into small squares for processing (Fig. 3c), achieved in a way similar to that described above, and STL model data recognizable by the printer were obtained. These data were then imported into the 3D printer, and the model was enlarged 20x for slicing, generating print paths. Finally, the model schematic of a single muscle was successfully printed, but it was distorted. Therefore, the CAD software (AutoCAD 2021, Autodesk Inc., USA) was considered for the construction of a fish flesh model for an appearance simulation.

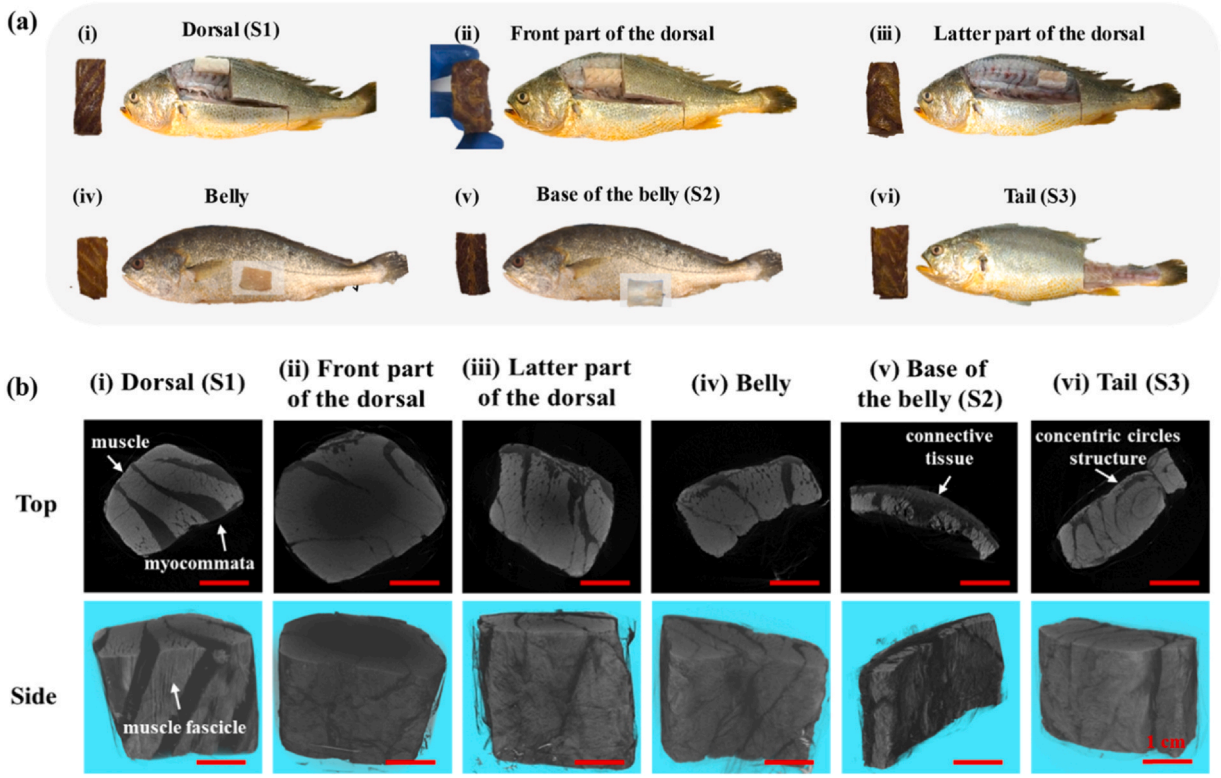


**Fig. 2.** Micro-CT scanning of different parts of yellow croaker fish muscle tissue. (a) Schematic diagram of sampling location and staining status of samples. (b) Sample status and Micro-CT imaging images by 10 μm precision. i, dorsal; ii, front part of the dorsal; iii, latter part of the dorsal; iv, belly; v, base of the belly; vi, tail. Red label, 1 cm.

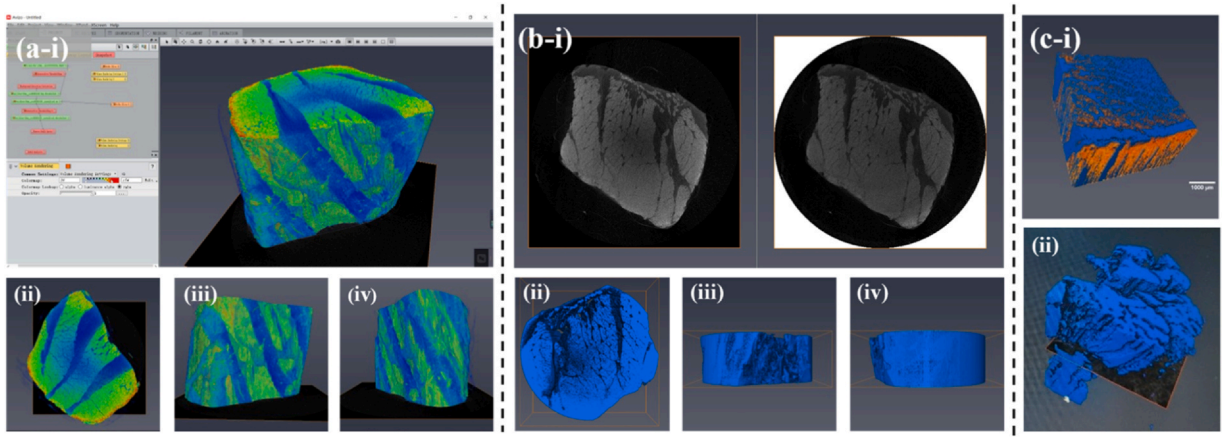


**Fig. 3.** Processing of the Micro-CT data of fish muscle tissue. (a) Rendering and coloring of the dorsal fish model: i, software page; ii-iv, three-dimensional views. (b) Preprocessing and model generation of CT data (the latter part of the dorsal flesh): i, preprocessing of color homogenization; ii-iv, three-dimensional views of model generation. (c) Fish localized STL data generation and 3D printing: i, CT model; ii, single muscle STL model generation.

The construction process is roughly as follows: (1) 2D wireframes of muscle/fat outlines are drawn according to high-precision CT scans; (2) the wireframes are closed to create a surface domain; (3) they are stretched into 3D solids; and (4) they are exported as STL models. In dual-nozzle 3D printing, the two models must be aligned with each other, and to facilitate the positioning of the printer, two small rectangular solids can be additionally created at the diagonal end of the single muscle/fat model, thus obtaining a composite model of fish tissue that can be used for 3D printing with a high degree of simulation (Fig. 4).

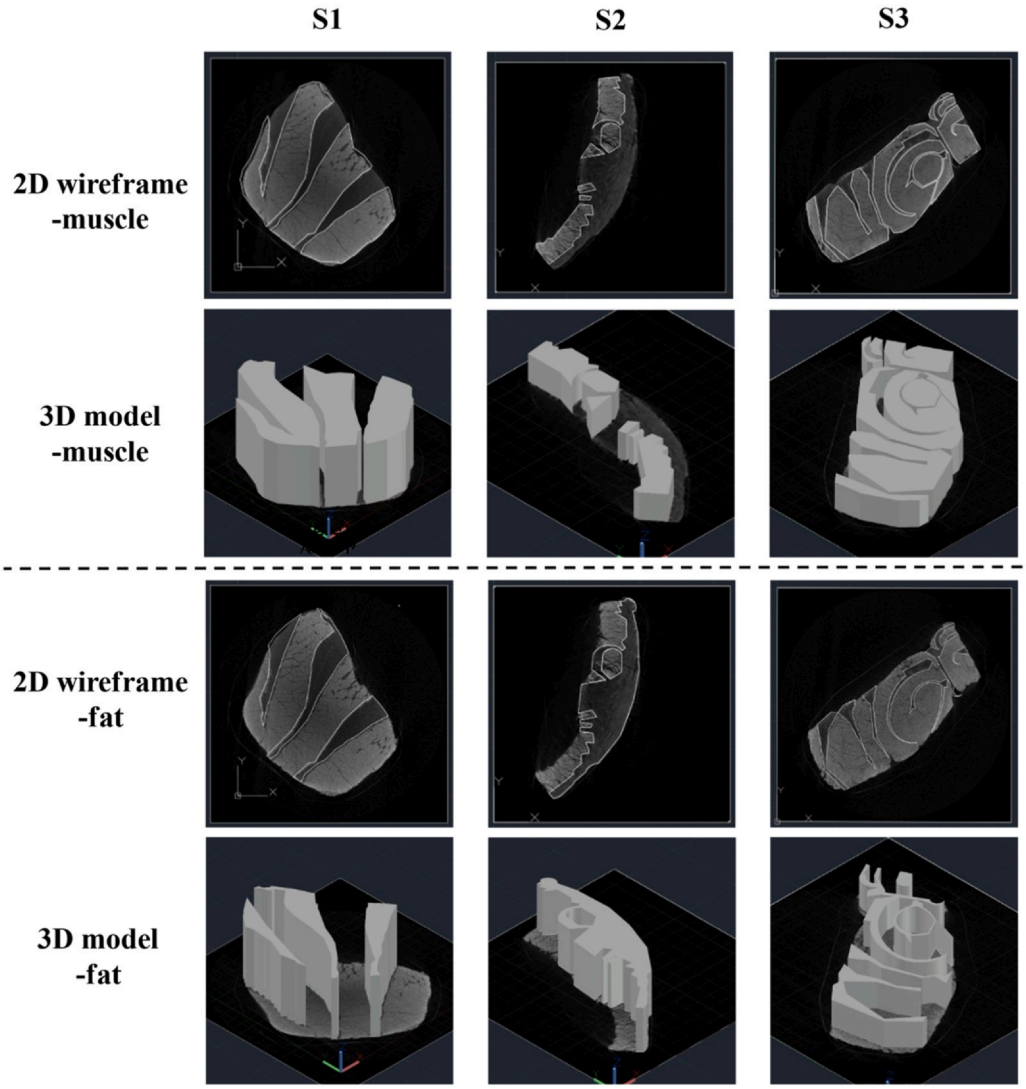


**Fig. 4.** High simulation CAD composite model of three parts of fish muscle tissue (S1-dorsal flesh; S2-the base of the belly flesh; S3-the tail).

### *3.3. Dual-nozzle 3D printing for plant-based fish muscle tissue*

As shown in Fig. 5a, the dual-nozzle printing method and software settings were first subjected to pre-experimental testing. The dual-nozzle 3D printing method follows that of Liu et al. [11], where two pre-designed independent 3D STL models sharing the same coordinates were created. The two STL files were then merged into one multi-material file and each file assigned to an extrusion unit (by one material).

After the dual-nozzle pre-experiment test to determine the basic printing parameters, the fish muscle/fat high simulation composite model created in part 3.2 is imported. Then, the corresponding parameters for slicing are set, as shown in Fig. 5b, and the printing parameters optimized and adjusted (e.g., manual calibration of the dual-nozzle offset, dual-nozzle moving rate matching, dual-nozzle air pressure adjustment, layer height, fill rate, slicing path settings), until successful printing.

If the slice path is adjusted from Grid mode to Rectilinear mode (as in the upper part of Fig. 5b-ii, applicable to the printing of back models with a greater number of straight lines) or Concentric mode (as in the lower part of Fig. 5b-ii, applicable to the printing of tail models with more rounded shapes), print molding accuracy can be improved (Fig. 5c), and the successful dual-nozzle printing parameters are shown in Table 1.

In accordance with the dual-nozzle 3D printing parameters in Table 1, the simulated fish meat of the three parts was printed, and the 3D model diagram and simulated fish meat printing effect are shown in Fig. 6a. As shown, the dual-nozzle 3D printing process after parameter adjustment can print the samples with a high printing accuracy. To compare visually the printing deviations in the simulated fish meat, the printing deformation rate can be calculated by measuring the length of the printed samples in the X, Y, and Z directions and comparing it with the printed preset model (Fig. 6b), where a deformation rate greater than 0 indicates that the

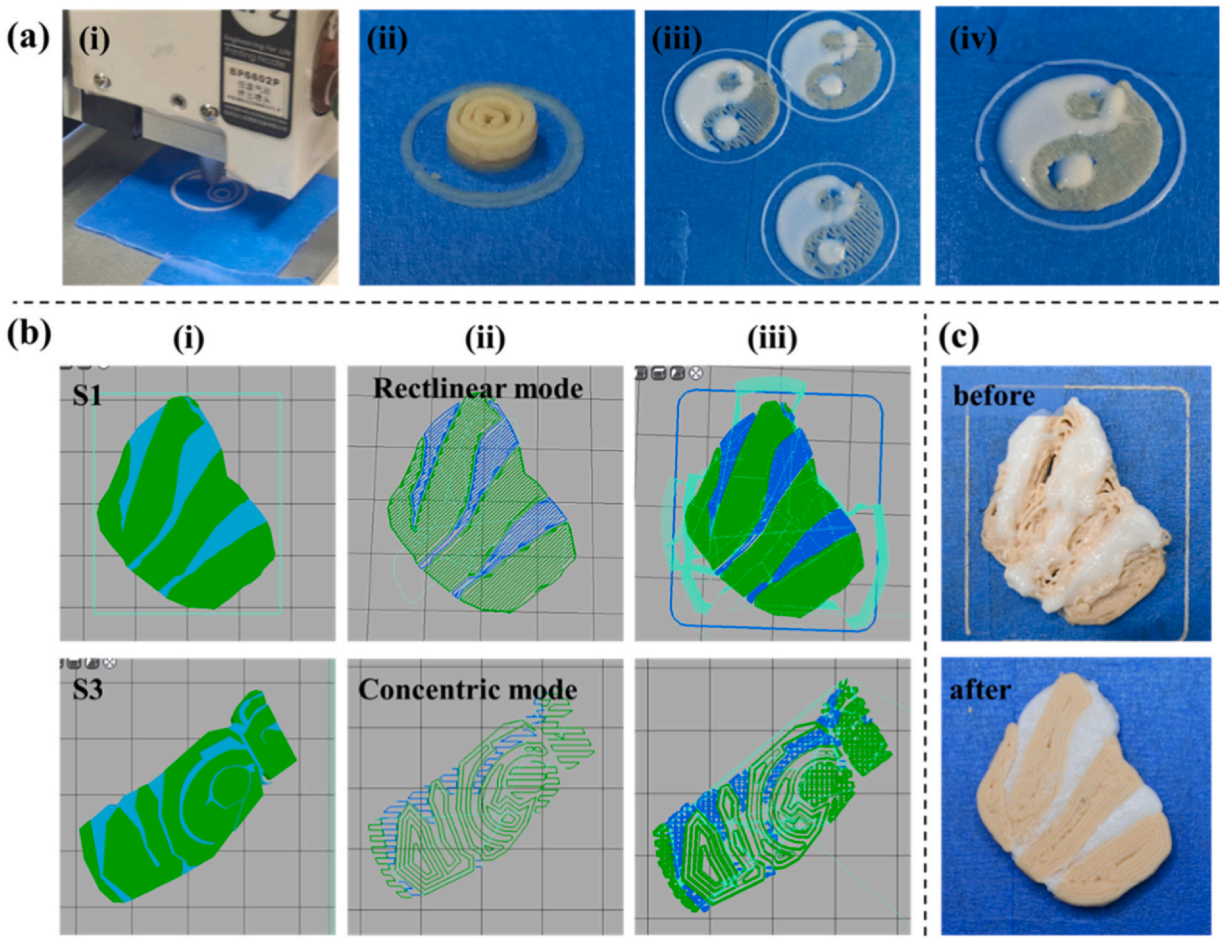


**Fig. 5.** Pretest and parameter adjustment for dual-nozzle extrusion printing. (a) Experimental test with dual nozzles (Tachi pattern): i-ii, single material printing; iii, dual-material printing; iv, optimized adjustment of parameters for dual nozzles. (b) Diagram of optimized adjustments for fish simulation printing with dual nozzles for represented fish tissue parts (S1-dorsal flesh; S3-the tail): i, print model; ii, printing path optimization (with different modes for S1 and S3); iii, total printing paths. (c) Comparison of printing effect before and after parameter adjustment using S1 as the case.

samples expand and a rate less than zero means they contract. The simulated fish flesh of the back and tail expanded in the X, Y and Z directions, and the simulated fish flesh of the abdomen contracted in all but the Y direction. According to the Eq. (2) of part 2.8, the printing control accuracy of the back-, abdomen-, and tail-simulated fish meat is calculated to be 93 %, 97 %, and 93 %, respectively, and the printing control accuracy of the simulated fish meat of the composite structure of the three parts reached more than 90 %, which is a good construction for the flesh simulation, incorporating the actual scene diagram shown in Fig. 6c.

### *3.4. Water state and distribution analysis of plant-based yellow croaker flesh tissue*

The moisture status of the plant-based yellow croaker muscle tissue was analyzed using low-field nuclear magnetic resonance (LF NMR) and compared with the real yellow croaker flesh (steamed), and the results are shown in Table 2 and Fig. 7. The transverse relaxation time ($T_2$) distribution can be computed using the T-invfit program to transform the exponentially decaying signal into a multi-exponential distribution [18]. In the multi-exponential fitting study, $A_{2i}$, $S_{2i}$, and $T_{2i}$ stand for the signal amplitude, percentage relative peak area, and transverse relaxation time of the i-th hydrogen proton state, respectively [3]. Tan et al. [16] report that the $T_2$ relaxation times ranged from 0.1 to 1, 1–10, 10–100, and 100–1000 ms for tightly bound water ($T_{2b}$), bound water ($T_{21}$), immobilized water ($T_{22}$), and free water ($T_{23}$), respectively.

According to Pearce et al. [12], there are four main fractions resulting in the presence of water in real fish flesh: one type of water is tightly bound, meaning charged hydrophilic groups firmly bind the water; another type is bound water, meaning charged hydrophilic groups combine with the water; a third type is immobilized water, meaning the molecular orientation toward the charged group is less orderly; and the fourth type is free water, meaning it is held only by capillary forces and its orientation is independent of the charged group.

Notably, as shown in Fig. 7, the real yellow croaker flesh and the plant-based yellow croaker flesh demonstrated three different water fractions: free water ($T_{23}$), immobilized water ($T_{22}$), and tightly bound water ($T_{2b}$). The flesh tissue of the yellow croaker

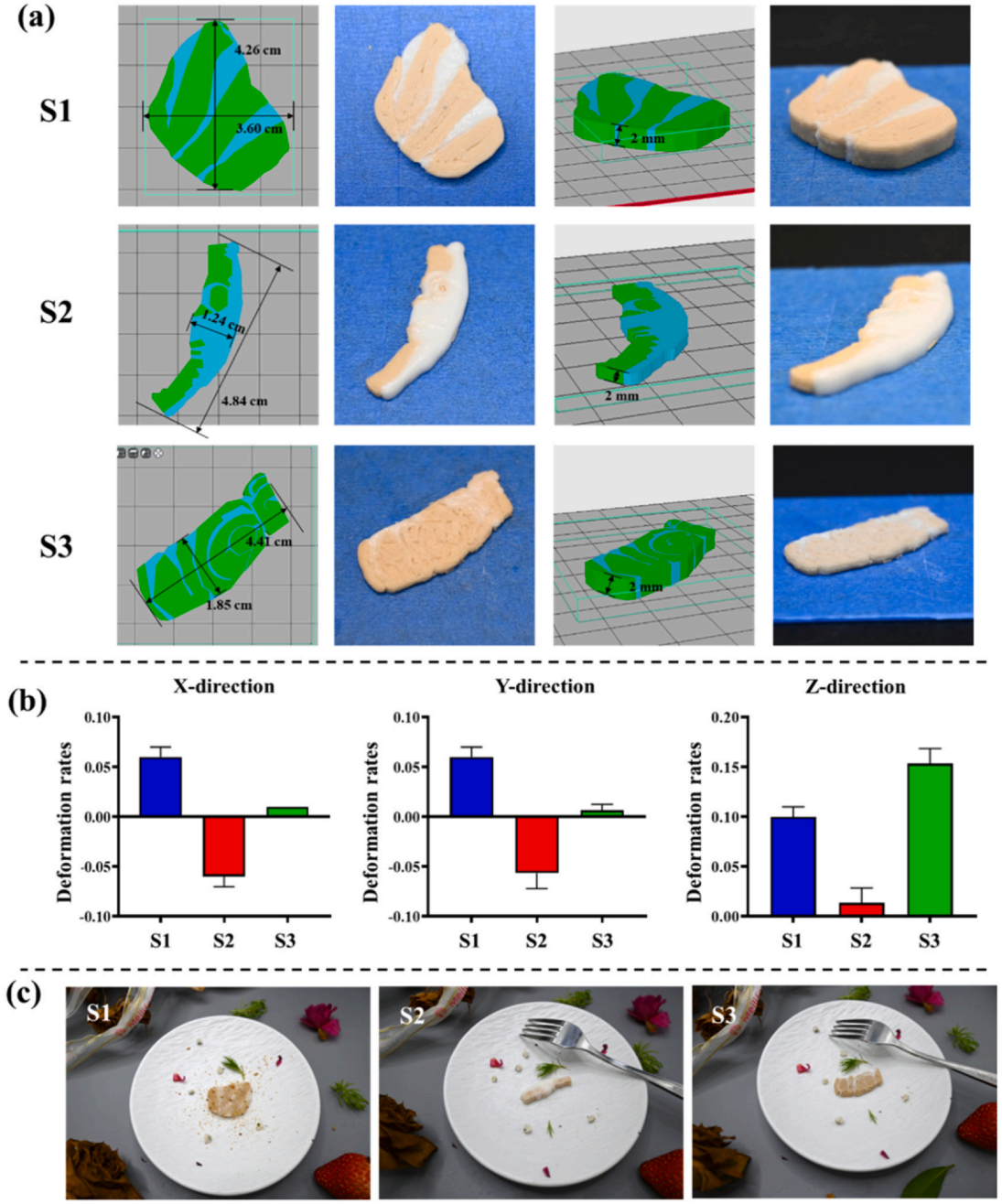


**Fig. 6.** Dual-nozzle 3D printing of plant-based yellow croaker muscle tissue (S1-dorsal flesh; S2-the base of the belly flesh; S3-the tail). (a) 3D model and plant-based yellow croaker flesh printing products; (b) Printed deformation rates of plant-based fish tissues in X/Y/Z directions; (c) Demonstration of practical application scenarios of plant-based yellow croaker analogs.

produced an excellent simulation, as the distribution and state of the water in the samples show the status of the diverse types of water. In all three parts (S1, S2, S3) of the plant-based flesh and real yellow croaker fish, the water component with the highest content is $T_{22}$, and its proportion ($S_{22}$) is about 90 %. In the S1 part, the lowest content of plant-based flesh and real yellow croaker fish is $T_{2b}$. In S2 and S3, the lowest content of plant-based flesh and real yellow croaker fish is $T_{23}$. These results show that plant-based flesh also exhibits the same phenomenon as the real yellow croaker fish, caused by different water component contents.

As shown in Fig. 7 and Table 2, in the multi-component analysis, the S3 part (the tail) has the best simulation effect on the content of each water fraction, and the peak area of each water fraction of the plant-based flesh (S3) is close to that of yellow croaker fish (S3). For example, the $S_{2b}$ of the plant-based flesh (S3) is 3.42 ± 0.47 %, while that of yellow croaker fish (S3) is 3.36 ± 0.57 %, demonstrating that the content of the two $T_{2b}$ fractions is proximate. The water that is tightly bound to muscle proteins ($T_{2b}$) gives the

**Table 2**
LF NMR relaxation information of yellow croaker flesh and plant-based yellow croaker fish tissues with different parts (S1-dorsal flesh; S2-the base of the belly flesh; S3-the tail).

| Sample | $T_{2b}$ (ms) | $S_{2b}$ (%) | $T_{22}$ (ms) | $S_{22}$ (%) | $T_{23}$ (ms) | $S_{23}$ (%) |
|---|---|---|---|---|---|---|
| Yellow croaker flesh (S1) | 0.38 ± 0.11 | 6.06 ± 0.87 | 37.65 ± 1.26 | 84.89 ± 5.85 | 705.48 ± 0.00 | 11.45 ± 1.25 |
| Plant-based flesh (S1) | 0.66 ± 0.04 | 3.82 ± 0.29 | 18.74 ± 0.65 | 89.03 ± 1.25 | 705.48 ± 0.00 | 9.29 ± 3.02 |
| Yellow croaker flesh (S2) | 0.54 ± 0.05 | 11.39 ± 1.29 | 12.33 ± 0.00 | 83.22 ± 2.24 | 811.13 ± 0.00 | 4.08 ± 2.30 |
| Plant-based flesh (S2) | 0.35 ± 0.08 | 3.74 ± 0.16 | 52.25 ± 4.30 | 94.18 ± 0.63 | 811.13 ± 0.00 | 2.08 ± 0.47 |
| Yellow croaker flesh (S3) | 0.60 ± 0.49 | 3.36 ± 0.57 | 52.25 ± 5.27 | 95.25 ± 1.15 | 851.62 ± 85.89 | 1.39 ± 0.58 |
| Plant-based flesh (S3) | 0.32 ± 0.05 | 3.42 ± 0.37 | 49.77 ± 0.00 | 94.66 ± 0.68 | 841.50 ± 60.74 | 1.92 ± 0.45 |

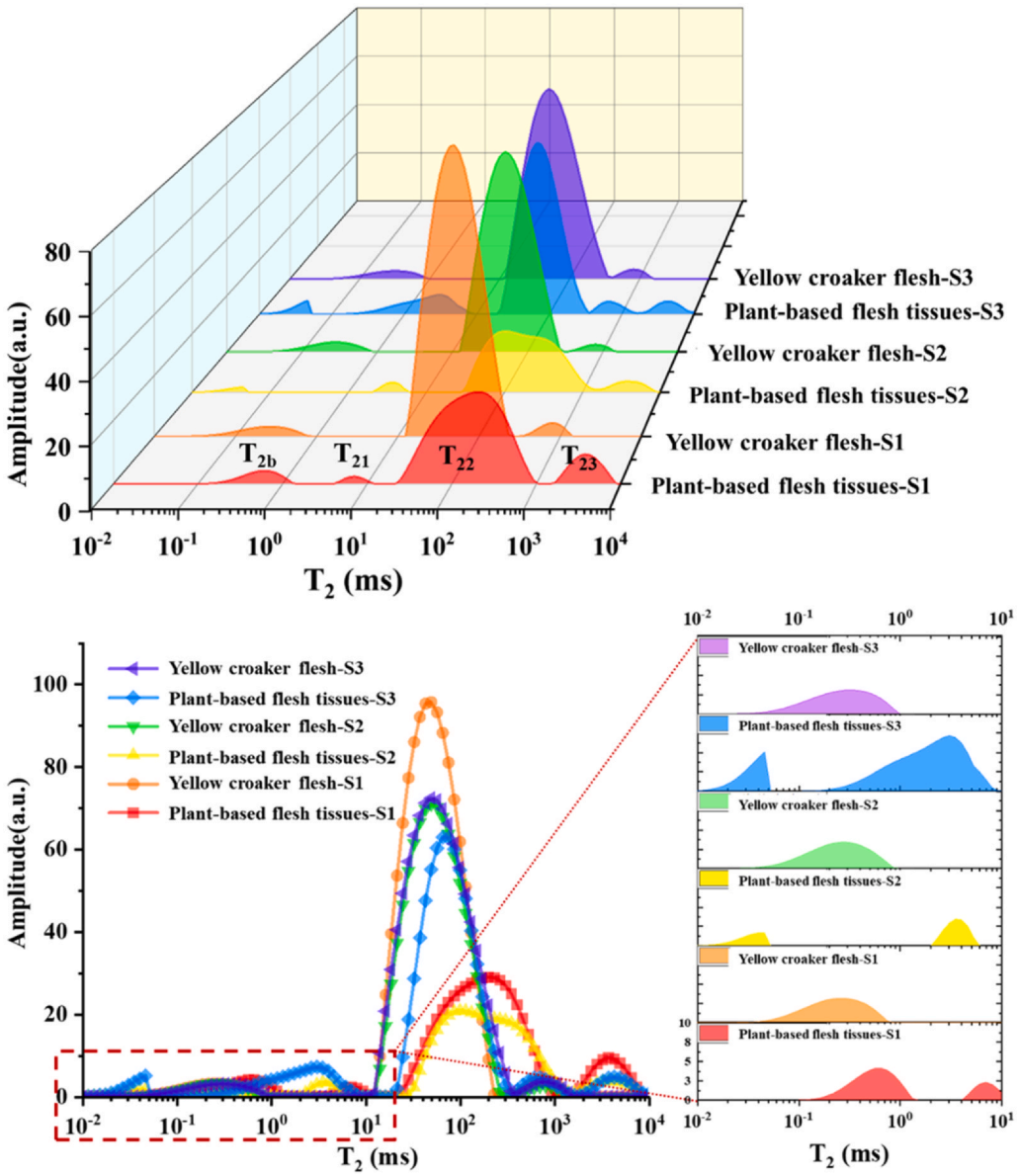


**Fig. 7.** LF NMR of plant-based yellow croaker muscle tissues (S1-dorsal flesh; S2-the base of the belly flesh; S3-the tail).

**Table 3**
TPA data of plant-based yellow croaker muscle tissues and yellow croaker flesh (steamed) with three parts (S1-dorsal flesh; S2-the base of the belly flesh; S3-the tail).

| Sample | Hardness/N | Springiness | Adhesiveness/gf-mm | Gumminess/gf | Resilience |
|---|---|---|---|---|---|
| Yellow croaker flesh (S1) | 7.04 ± 1.77 | 0.58 ± 0.09 | 2.21 ± 0.93 | 321.85 ± 113.66 | 0.27 ± 0.06 |
| Plant-based flesh (S1) | 10.48 ± 2.01 | 0.78 ± 0.19 | 2.26 ± 0.72 | 445.47 ± 223.38 | 0.35 ± 0.05 |
| Yellow croaker flesh (S2) | 9.07 ± 3.18 | 0.70 ± 0.1 | 1.43 ± 0.84 | 659.88 ± 227.67 | 0.49 ± 0.07 |
| Plant-based flesh (S2) | 12.0 ± 1.80 | 0.64 ± 0.04 | 2.75 ± 0.54 | 460.34 ± 90.76 | 0.45 ± 0.16 |
| Yellow croaker flesh (S3) | 6.64 ± 2.69 | 0.74 ± 0.06 | 1.28 ± 1.11 | 454.11 ± 208.08 | 0.58 ± 0.22 |
| Plant-based flesh (S3) | 3.63 ± 0.43 | 0.65 ± 0.21 | 3.51 ± 0.23 | 327.01 ± 14.42 | 0.38 ± 0.02 |

meat its firm texture and is closely linked to the meat's tenderness and juiciness when consumed [12]. $T_{2b}$ fractions appeared in both simulated and real yellow croaker flesh with similar content (especially in the abdomen), and this result proved that the plan-based fish meat had a good simulation effect.

### 3.5. Textural analysis of plant-based yellow croaker flesh tissue

The simulated fish meat underwent a texture profile analysis (TPA), and the results are shown in Table 3. Hardness is the force that prevents deformation, i.e., the force required to compress a substance between the molars (solid) or between the tongue and the palate (semi-solid) [15]. Meanwhile, gumminess is the energy required to break down semi-solid food into a state conducive to swallowing; it is the result of low hardness and high viscosity [20]. Further, adhesiveness is a force that overcomes the attraction between the surface of the food and the surface of other materials with which the food comes into contact, and it represents the force that removes food debris adhering to the palate of the mouth during normal eating [4].

The hardness data of the simulations of all three parts (the dorsal flesh [S1], the base of the belly flesh [S2], and the tail [S3]) still feature a certain difference from real yellow croaker fish. The hardness of the yellow croaker fish (S1) is 7.04 ± 1.77 N, and the hardness of the plant-based flesh (S1) is 10.48 ± 2.01 N; thus, the hardness of simulated fish in S1 is about 3 N larger than that of real fish. In addition, the hardness of the yellow croaker fish (S2) is 9.07 ± 3.18 N, and the hardness of the plant-based flesh (S2) is 12.0 ± 1.80 N; therefore, the hardness of simulated fish in S2 is also about 3 N larger than that of real fish. Finally, the hardness of the yellow croaker fish (S3) is 6.64 ± 2.69 N, and the hardness of the plant-based flesh (S3) is 3.63 ± 0.43 N. However, unlike S1 and S2, the real fish in S3 is 3 N harder than the simulated fish. In all three parts (S1, S2, S3), the hardness difference between plant-based flesh and real fish was about 3 N, which showed some common regularity, likely due to the hardness limitation of the plant-based materials themselves. Anyway, there is still a certain gap between the hardness of simulated fish and that of real fish, and the formula may continue to be adjusted to obtain better simulation results.

Some TPA data of the simulated and real fish meat for all three parts (S1, S2, and S3) are relatively close to each other, within the margin of error, especially for springiness and resilience. Meanwhile, the rate at which an object returns to its undeformed state after the deforming force has disappeared is known as springiness, and in the case of food consumption, springiness is considered the extent to which food returns to its original state after being squeezed by the teeth [10]. In the three parts of real yellow croaker fish flesh, the springiness is 0.58 (S1), 0.70 (S2), and 0.74 (S3), respectively, while the corresponding elasticity of the simulated fish is 0.78 (S1), 0.64 (S2), and 0.65 (S3), respectively. In addition to that of the S1 part, the elasticity of the S2 and S3 parts of the simulated fish is remarkably close to that of real yellow fish. In addition, a crisp, elastic, and smooth texture is important to fish flesh, and the above results indicate that the simulated fish meat with a composite structure prepared by 3D printing has similar textural properties to real fish meat, to some extent.

### 3.6. Nutrition analysis of plant-based yellow croaker flesh tissue

The back is the most frequently consumed part of a fish in daily life due to fewer spines and firmer meat, so the simulated fish back meat was used as a representative here. The simulated fish dorsal meat tissue obtained by dual-nozzle 3D printing was analyzed in comparison with the dorsal muscle of real yellow croaker flesh for nutrient content, and the results are shown in Table 4. The crude protein content of yellow croaker flesh (dorsal-S1) was 18.47 ± 0.45 g/100 g, while the crude protein content of the experimentally produced simulated fish flesh (S1) was 12.75 ± 0.29 g/100 g, with a similarity of 69.03 %. The crude fat content of the yellow croaker dorsal flesh was 7.67 ± 0.25 g/100 g, while that of the plant-based simulated fish flesh (S1) obtained by 3D printing was 3.90 ± 0.1 g/100 g, with a similarity of 50.85 %. Thus, the crude protein and crude fat of the plant-based yellow croaker flesh tissue prepared using 3D printing technology were slightly lower than those of real fish flesh.

Concerning amino acid composition, the top four amino acids in yellow croaker (S1) were glutamic acid, aspartic acid, lysine, and leucine, while the top four amino acids in simulated fish meat (S1) were glutamic acid, aspartic acid, leucine, and lysine, with aspartic acid having the highest similarity at 98.11 %. The eight essential amino acids required by the human body are lysine, methionine (methionine), leucine, isoleucine, phenylalanine, threonine, tryptophan, and valine. Except for tryptophan, which was not measured due to the limitations of the analytical method, the contents of the seven essential amino acids required by the human body in simulated fish products were similar to those of real fish. Among all amino acid species, most of the amino acid contents were more than 50 % similar, indicating that the amino acid composition of the simulated fish meat prepared using 3D printing technology was highly similar to that of real fish meat, and the aim of replacing fish protein could be potentially realized. Regarding the fatty acid

**Table 4**
Nutrition information of yellow croaker dorsal flesh and plant-based yellow croaker dorsal flesh tissues (S1-dorsal flesh).

| Content (g/100 g) | Yellow croaker flesh (S1) | Plant-based muscle tissues (S1) | Relative Proportion (%) | Content (g/100 g) | Yellow croaker flesh (S1) | Plant-based muscle tissues (S1) | Relative Proportion (%) |
|---|---|---|---|---|---|---|---|
| Crude protein | 18.47 ± 0.45 | 12.75 ± 0.29 | 69.03 | C14:0 | 0.16 ± 0.00 | 0.38 ± 0.00 | 237.50 |
| Crude fat | 7.67 ± 0.25 | 3.90 ± 0.01 | 50.85 | C14:1 | | | |
| Asp | 1.59 ± 0.00 | 1.62 ± 0.00 | 101.89 | C15:0 | 0.03 ± 0.00 | 0.01 ± 0.00 | 33.33 |
| Thr | 0.68 ± 0.01 | 0.55 ± 0.00 | 80.88 | C15:1 | | | |
| Ser | 0.62 ± 0.00 | 0.70 ± 0.00 | 87.10 | C16:0 | 1.52 ± 0.00 | 0.63 ± 0.00 | 41.45 |
| Glu | 2.45 ± 0.01 | 2.59 ± 0.01 | 105.71 | C16:1 | 0.53 ± 0.00 | 0.47 ± 0.00 | 88.68 |
| Gly | 0.84 ± 0.00 | 0.57 ± 0.00 | 67.86 | C17:0 | 0.03 ± 0.00 | 0.01 ± 0.00 | 33.33 |
| Ala | 1.04 ± 0.00 | 0.60 ± 0.00 | 57.69 | C17:1 | | | |
| Cys | 0.077 ± 0.00 | | | C18:0 | 0.31 ± 0.00 | 0.12 ± 0.00 | 38.71 |
| Val | 0.78 ± 0.01 | 0.74 ± 0.01 | 94.87 | C18:1n9t | | | |
| Met | 0.30 ± 0.01 | 0.11 ± 0.00 | 36.67 | C18:1n9c | 1.26 ± 0.01 | 0.54 ± 0.00 | 42.86 |
| Ile | 0.59 ± 0.00 | 0.73 ± 0.00 | 123.73 | C18:2n6c | 0.18 ± 0.00 | 0.35 ± 0.00 | 194.44 |
| Leu | 1.22 ± 0.01 | 1.14 ± 0.01 | 93.44 | C20:0 | 0.01 ± 0.00 | | |
| Tyr | 0.40 ± 0.00 | 0.55 ± 0.00 | 137.50 | C18:3n3 | 0.03 ± 0.00 | 0.04 ± 0.00 | 133.33 |
| Phe | 0.65 ± 0.00 | 0.75 ± 0.00 | 115.38 | C20:1 | 0.08 ± 0.00 | 0.02 ± 0.00 | 25.00 |
| His | 0.27 ± 0.00 | 0.56 ± 0.00 | 207.41 | C20:2 | 0.01 ± 0.00 | 0.02 ± 0.00 | 200.00 |
| Lys | 1.49 ± 0.01 | 0.94 ± 0.01 | 63.09 | C20:3n6 | 0.01 ± 0.00 | | |
| Arg | 0.93 ± 0.00 | 1.03 ± 0.01 | 110.75 | C20:3n3 | | | |
| Pro | 0.44 ± 0.01 | 0.76 ± 0.00 | 172.72 | C20:4n6 | 0.10 ± 0.00 | 0.02 ± 0.00 | 20.00 |
| C4:0 | | | | C22:1n9 | 0.01 ± 0.00 | | |
| C6:0 | | | | C23:0 | | | |
| C8:0 | | | | C22:2 | | 0.01 ± 0.00 | |
| C10:0 | | | | C20:5n3 (EPA) | 0.14 ± 0.00 | 0.04 ± 0.00 | 28.57 |
| C11:0 | | | | C24:0 | 0.01 ± 0.00 | | |
| C12:0 | | 0.01 ± 0.00 | | C24:1 | 0.04 ± 0.00 | | |
| C13:0 | | | | C22:6n3 (DHA) | 0.36 ± 0.00 | 0.34 ± 0.00 | 94.44 |

composition, the highest content of both yellow croaker meat (S1) and simulated fish flesh (S1) was C16:0 (methyl palmitate). In addition, the DHA content of the simulated fish meat product (0.34 g/100 g) produced in this study was 94.4 %, similar to that of real yellow croaker meat (0.36 g/100 g), which clearly meets the requirements for fish-specific nutrient intake.

## 4. Conclusions

In this study, plant-based simulated yellow croaker meat tissues were prepared by dual-nozzle 3D printing using simulated muscle and fat materials as printing inks. Based on the micro-CT scanning data, a muscle/fat biphasic high simulation model for 3D printing yellow croaker meat in three parts (the dorsal, the base of the belly flesh, and the tail) was successfully constructed via CAD reconstruction. The printing process was optimized and adjusted by controlling the dual-nozzle printing process parameters (including manual calibration of the dual-nozzle offset, layer height, fill rate, printing speed, air pressure, etc.); finally, a dual-nozzle 3D-printed product of plant-based fish flesh was successfully created, with a printing accuracy of more than 90 % for the composite structure. Overall, it was found that the texture characteristics, moisture distribution, and content of many nutrients in simulated fish were close to those of real fish.

## CRediT authorship contribution statement

**Donghong Liu:** Writing – review & editing, Methodology. **Enbo Xu:** Writing – review & editing, Supervision, Funding acquisition. **Jie Li:** Writing – original draft, Resources, Methodology, Investigation, Conceptualization. **Haohao Hu:** Validation, Software, Formal analysis. **Ruihao Niu:** Writing – original draft, Resources, Methodology, Investigation, Formal analysis. **Qingqing Zhu:** Resources, Methodology, Investigation, Formal analysis. **Siyu Yao:** Resources, Methodology, Investigation, Formal analysis. **Jianwei Zhou:** Writing – review & editing, Methodology.

## Declaration of Competing Interest

Donghong Liu is an Associate Editor for Food Physics and was not involved in the editorial review or the decision to publish this article. All other authors declare that there are no competing interests.

## Acknowledgements

This work was supported by the National Key Research and Development Program of China (2022YFF1101800), the Natural Science Foundation of China (32272464), and the Young Elite Scientists Sponsorship Program by CAST (2022QNRC001). We also thank the Project Supported by the Scientific Research Fund of Zhejiang Provincial Education Department (Y202250812).

## References

[1] N. Alexandratos, J. Bruinsma, World Agriculture towards 2030/2050: The 2012 Revision, ESA Working paper, Rome, 2012.
[2] C.M. Anderson, M.J. Krigbaum, M.C. Arostegui, M.L. Feddern, J.Z. Koehn, P.T. Kuriyama, C. Morrisett, C.I. Allen Akselrud, M.J. Davis, C. Fiamengo, A. Fuller, Q. Lee, K.N. McElroy, M. Pons, J. Sanders, How commercial fishing effort is managed, Fish Fish *20* (2) (2018) 268–285.
[3] I.G. Aursand, U. Erikson, E. Veliyulin, Water properties and salt uptake in Atlantic salmon fillets as affected by ante-mortem stress, rigor mortis, and brine salting: A low-field $^{1}$H NMR and 1H/23Na MRI study, Food Chem. *120* (2) (2010) 482–489.
[4] J.H. Cheng, D.W. Sun, Z. Han, X.A. Zeng, Texture and structure measurements and analyses for evaluation of fish and fillet freshness quality: A review, Compr. Rev. Food Sci. Food Saf. *13* (1) (2014) 52–61.
[5] M. Eriksen, L.C.M. Lebreton, H.S. Carson, M. Thiel, C.J. Moore, J.C. Borerro, F. Galgani, P.G. Ryan, J. Reisser, Plastic Pollution in the World's Oceans: More than 5 Trillion Plastic Pieces Weighing over 250,000 Tons Afloat at Sea, Plos One *9* (12) (2014) e111913.
[6] M.D. Hiran, Fish Morphology, CRC Press, 2017.
[7] N.S. Jeffery, R.S. Stephenson, J.A. Gallagher, J.C. Jarvis, P.G. Cox, Micro-computed tomography with iodine staining resolves the arrangement of muscle fibres, J. Biomech. *44* (1) (2011) 189–192.
[8] H.J. Ko, Y. Wen, J.H. Choi, B.R. Park, H.W. Kim, H.J. Park, Meat analog production through artificial muscle fiber insertion using coaxial nozzle-assisted three-dimensional food printing, Food Hydrocoll. *120* (2021) 106898.
[9] J. Li, R. Niu, Q. Zhu, S. Yao, J. Zhou, W. Wang, Q. Chen, J. Yin, D. Liu, E. Xu, Nanostarch-enhanced 3D printability of carrageenan emulsion gel for high-fidelity and nutrition-fortified fish fat mimics, Food Hydrocoll. *145* (2023) 109099.
[10] A. Listrat, B. Lebret, I. Louveau, T. Astruc, M. Bonnet, L. Lefaucheur, B. Picard, J. Bugeon, How muscle structure and composition influence meat and flesh quality, Sci. World J. *2016* (2016) 1–14.
[11] Z. Liu, M. Zhang, C. Yang, Dual extrusion 3D printing of mashed potatoes/strawberry juice gel, LWT *96* (2018) 589–596.
[12] K.L. Pearce, K. Rosenvold, H.J. Andersen, D.L. Hopkins, Water distribution and mobility in meat during the conversion of muscle to meat and ageing and the impacts on fresh meat quality attributes — A review, Meat Sci. *89* (2) (2011) 111–124.
[13] S. Ruan, J. Tang, Y. Qin, J. Wang, T. Yan, J. Zhou, D. Gao, E. Xu, D. Liu, Mechanical force-induced dispersion of starch nanoparticles and nanoemulsion: Size control, dispersion behaviour, and emulsified stability, Carbohydr. Polym. *275* (2022) 118711.
[14] H. Shi, J. Li, E. Xu, H. Yang, D. Liu, J. Yin, Microscale 3D printing of fish analogues using soy protein food ink, J. Food Eng. *347* (2023) 111436.
[15] S.A. Szczesniak, Texture is a sensory property, Food Qual. Prefer. *13* (4) (2002) 215–225.
[16] M. Tan, Z. Lin, Y. Zu, B. Zhu, S. Cheng, Effect of multiple freeze-thaw cycles on the quality of instant sea cucumber: Emphatically on water status of by LF NMR and MRI, Food Res. Int. *109* (2018) 65–71.
[17] Y. Wang, W.Y. D.H., Y.H. Xiong, High internal phase emulsions of ω-3 fatty acids stabilized by fish scale gelatin, Food Hydrocoll. (2023) 109254.
[18] C. Wang, X. Wang, C. Liu, C. Liu, Application of LF NMR to the characterization of camellia oil-loaded pickering emulsion fabricated by soy protein isolate, Food Hydrocoll. *112* (2021) 106329.
[19] E. Xu, R. Niu, J. Lao, S. Zhang, J. Li, Y. Zhu, H. Shi, Q. Zhu, Y. Chen, Y. Jiang, W. Wang, J. Yin, Q. Chen, X. Huang, J. Chen, D. Liu, Tissue-like cultured fish fillets through a synthetic food pipeline, Npj Sci. Food *7* (1) (2023) 17.
[20] C. Yuan, D. Xu, B. Cui, Y. Wang, Gelation of κ-carrageenan/Konjac glucommanan compound gel: Effect of cyclodextrins, Food Hydrocoll. *87* (2019) 158–164.
[21] L. Zhou, R. Zhou, X. Xie, F. Yin, Characteristics and risk assessment of cryptocaryoniasis in large yellow croaker (Larimichthys crocea) at different densities in industrialized aquaculture, Aquaculture *582* (2024).
[22] Y. Zhu, E. Xu, J. Yin, W. Xu, D. Liu, Visualization, modeling and analysis of salmon muscle structure: Based on micro-CT, Food Struct. *37* (2023) 100325.